JOURNAL OF SOLID STATE CHEMISTRY 41, 272–276 (1982)

Structural and Magnetic Properties of $KPbCr_2F_9$

M. VLASSE, J. P. CHAMINADE, J. M. DANCE, M. SAUX, AND P. HAGENMULLER

Laboratoire de Chimie du Solide du CNRS, Université de Bordeaux I, 351 cours de la Libération, 33405 Talence, France

Received July 8, 1981; in revised form October 22, 1981

A precise structural determination of $KPbCr_2F_9$ was carried out. The symmetry is orthorhombic with $a = 9.81(5)$, $b = 5.412(3)$, $c = 13.93(1)$ Å, and *Pnma*. The structure was refined from 1285 X-ray reflections by full-matrix least squares to an $R = 0.041$. The lattice is made up of double chains $(Cr_2F_9)_n^{3n-}$ running along the b axis with Pb and K atoms ensuring its cohesion. The results of the magnetic studies are reported and discussed.

Introduction

In the study of the system K–Ta–O–F a number of phases were isolated, in particular $K_2Ta_2O_3F_6$ (*1*). The determination of its structure has shown that it is made up of double infinite zigzag chains along the b axis. These chains are formed by $(TaO_3F_3)^{4-}$ octahedra sharing three oxygen corners belonging to the same face. The K^+ ions ensure the cohesion of the lattice (*2*).

The particular character of this structure led us to prepare isostructural, but entirely fluorinated compounds, using the experience of the laboratory in this field (*3–5*). We therefore prepared $KPbCr_2F_9$ and found that it was isostructural with the oxide fluoride. A precise structural determination was undertaken.

Moreover, the double-chain character of such a phase, structurally intermediate between a layer and a simple chain structure, gave further interest, since it could allow one to determine whether the magnetic interactions had also an intermediate character between the elementary 2D and 1D models. A study of the magnetic properties of $KPbCr_2F_9$ was also undertaken.

Experimental

Preparation

Powder samples were prepared by direct synthesis from KF, PbF_2, and CrF_3 in stoichiometric amounts heated to 650°C in a sealed gold tube for 40 hr. Single crystals were grown in a $PbCl_2$ flux at 870°C and cooled at a rate of 2°C/hr to 600°C. The color of both single crystals and powder was light green with a powder size of about 10 μm. No analysis was carried out except for a control on the iron content by Mössbauer spectroscopy, which indicated its total absence.

X-Ray Diffraction

Weissenberg and precession photographs indicate orthorhombic symmetry. The systematic extinctions are consistent with space groups $Pn2_1a$ and *Pnma*. The lattice

0022-4596/82/030272-05$02.00/0

TABLE I

POSITIONAL AND THERMAL PARAMETERS FOR $KPbCr_2F_9$ (SD ARE GIVEN IN PARENTHESES)

Atom	Site	x	y	z	$U_{11} \times 10^4$ (Å²)	U_{22}[a]	U_{33}	U_{13}	B (Å²)
K	4*c*	0.2703(4)	3/4	0.2975(2)	241(15)	175(15)	142(12)	34(11)	1.47((5)
Pb	4*c*	0.4449(5)	1/4	0.1105(4)	90(1)	1892(2)	114(2)	3(2)	1.03(1)
Cr(1)	4*c*	0.0669(2)	1/4	0.1559(1)	37(6)	1075(8)	55(6)	8(5)	0.52(2)
Cr(2)	4*c*	0.2307(2)	3/4	0.0076(1)	43(6)	85(8)	61(7)	2(5)	0.49(2)
F(1)	4*c*	0.2440(7)	1/4	0.2086(7)					1.73(10)
F(2)	4*c*	0.1513(7)	1/4	0.6122(8)					2.17(10)
F(3)	8*d*	0.0142(6)	0.4859(13)	0.2469(5)					1.33(10)
F(4)	8*d*	0.1575(7)	0.4916(12)	0.4492(5)					1.40(10)
F(5)	4*c*	0.3850(8)	1/4	0.3963(6)					1.45(10)
F(6)	8*d*	0.1213(7)	0.4992(16)	0.0659(5)					2.27(10)

[a] The anisotropic thermal coefficients are given by: $T = \exp[-2\pi^2(U_{11}h^2a^{*2} + U_{22}k^2b^{*2} + U_{33}l^2c^{*2} + 2U_{13}hla^*c^*)]$.

TABLE II

DISTANCES (Å) AND ANGLES (°) IN $KPbCr_2F_9$ (SD IN PARENTHESES)

		Cr(1) octahedral environment			
2 Cr(1)–F(3)	1.872(7)	F(3)–F(6)	2.732(10)	F(3)–Cr(1)–F(3)	95.52(5)
2 Cr(1)–F(6)	1.917(7)	F(3)–F(1)	2.645(9)	F(3)–Cr(1)–F(1)	89.48(5)
Cr(1)–F(1)	1.887(5)	F(3)–F(3)	2.553(10)	F(3)–Cr(1)–F(5)	90.00(5)
Cr(1)–F(5)	1.927(5)	F(3)–F(5)	2.686(8)	F(1)–Cr(1)–F(5)	179.30(5)
⟨Cr(1)–F⟩	1.899	F(6)–F(1)	2.687(9)	F(3)–Cr(1)–F(6)	178.20(5)
⟨Cr(1)–F_T⟩	1.877	F(6)–F(5)	2.733(9)	F(6)–Cr(1)–F(6)	89.50(5)
⟨Cr(1)–F_B⟩	1.920	F(6)–F(6)	2.697(10)	F(6)–Cr(1)–F(5)	90.60(5)
		⟨F–F⟩	2.676	F(6)–Cr(1)–F(1)	89.90(5)
				F(3)–Cr(1)–F(6)	170.70(5)
				Cr(1)–F(5)–Cr(2)	152.50(4)
				Cr(1)–F(6)–Cr(2)	159.00(4)
		Cr(2) octahedral environment			
2 Cr(2)–F(6)	1.912(7)	F(6)–F(2)	2.691(10)	F(6)–Cr(2)–F(6)	90.50(5)
2 Cr(2)–F(4)	1.890(6)	F(6)–F(6)	2.715(10)	F(6)–Cr(2)–F(2)	90.96(5)
Cr(2)–F(2)	1.862(7)	F(6)–F(5)	2.726(9)	F(6)–Cr(2)–F(5)	90.61(5)
Cr(2)–F(5)	1.922(5)	F(6)–F(4)	2.711(10)	F(6)–Cr(2)–F(4)	90.99(5)
⟨Cr(2)–F⟩	1.898	F(2)–F(4)	2.621(9)	F(2)–Cr(2)–F(5)	177.77(5)
⟨Cr(2)–F_T⟩	1.881	F(4)–F(4)	2.615(10)	F(4)–Cr(2)–F(4)	87.54(5)
⟨Cr(2)–F_B⟩	1.915	⟨F–F⟩	2.680	F(4)–Cr(2)–F(2)	88.59(5)
				F(4)–Cr(2)–F(5)	89.80(5)
				F(6)–Cr(2)–F(4)	178.53(5)
K environment				Pb environment	
2 K–F(3)	2.975(7)			2 Pb–F(3)	2.457(7)
2 K–F(3)	2.855(7)			Pb–F(1)	2.398(5)
2 K–F(1)	2.987(6)			2 Pb–F(2)	2.866(7)
K–F(2)	2.693(7)			2 Pb–F(4)	2.599(7)
2 K–F(4)	2.766(7)			2 Pb–F(4)	2.831(7)
⟨K–F⟩	2.873			⟨Pb–F⟩	2.656

parameters refined from single crystal data are a = 9.812(5), b = 5.412(3), and c = 13.93(1) Å. The cell contains four formula units [$d_{exp.}$ = 4.680(5), $d_{calcd.}$ = 4.679 g · cm^{-3}]. For $K_2Ta_2O_3F_6$ the space group is *Pnma* and the cell parameters are similar.

The intensities were collected on an Enraf–Nonius CD-3 three-circle automatic diffractometer with Mo$K\alpha$ monochromatic radiation (λ = 0.70942 Å). The single crystal in the form of a rectangular block 0.045 × 0.16 × 0.035 mm^3 was mounted along the b axis (0.16 mm). A total of 1285 independent reflections ($2\theta_{max}$ = 70°) had $I > 3\sigma(I)$ and were considered to be observed. These intensities were corrected for Lorentz and polarization effects, but not for absorption ($\mu r_{max} \simeq 2.4$).

The structure was solved using a 3D Patterson synthesis. The F atoms were located in a difference synthesis at an intermediate stage of the refinement. This refinement was carried out in space group *Pnma* as indicated by a centric distribution of the intensities. The same group was also retained for the $K_2Ta_2O_3F_6$ phase. Full-matrix least-squares anisotropic refinement (heavy atoms only) reduced $R = \Sigma||F_0| - |F_c||/\Sigma|F_0|$ to 0.041, based on a data-to-parameter ratio of 18.4:1 (*6*). A final ($F_0 - F_c$) synthesis confirmed the proposed solution.

$\Sigma w(|F_0| - |F_c|)^2$ was minimized with w taken as unity for all reflections. The overall scale factor was 1.847 ($F_0 = KF_c$). The form factors for K^+, Pb^{2+}, Cr^{3+}, and F^- were taken from McMaster *et al.* (*7*), with real and imaginary anomalous dispersion terms given by Cromer (*8*). The final atomic and thermal parameters are given in Table I. Table II contains the interatomic distances and angles. A table giving the calculated and observed structure amplitudes may be obtained on request from one of the authors (M.V.).

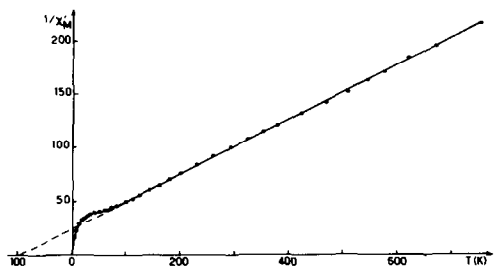

FIG. 1. Reciprocal magnetic susceptibility for $KPbCr_2F_9$.

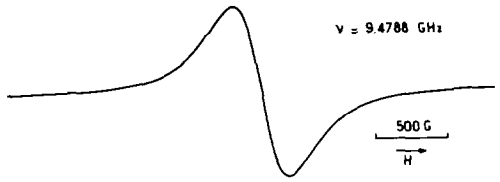

FIG. 2. EPR spectrum taken at 142 K.

Magnetic and EPR Measurements

The magnetic susceptibility data were obtained between 4.2 and 760 K using a Faraday balance calibrated with $Gd_2(SO_4)_3 \cdot 8H_2O$. Temperature was controlled by an AsGa probe in the range 4.2–300 K and by a Cr–Al thermocouple in the range 300–760 K. The thermal variation of the reciprocal molar susceptibility corrected for the diamagnetic contribution of the various atoms present ($\chi'_{M^{-1}}$) is given in Fig. 1.

The EPR spectrum was determined with a Brucker ER 200 tt spectrometer working in the X band (9.75 GHz) using a TE 102 cavity. The magnetic field ranging from 400 to 8000 G was measured with a proton NMR probe. The frequency was determined with a HP 5342 A frequency counter with a precision of about 1 kHz (relative precision: 10^{-6}). A continuous-flow Oxford Instruments cryostat provided the required temperatures between 4.2 and 300 K. Temperature was controlled by a Au–Fe thermocouple.

Between 19 and 300 K the spectrum has an isotropic lineshape given in Fig. 2. Below 19 K the line broadens considerably and finally disappears. The line is symmet-

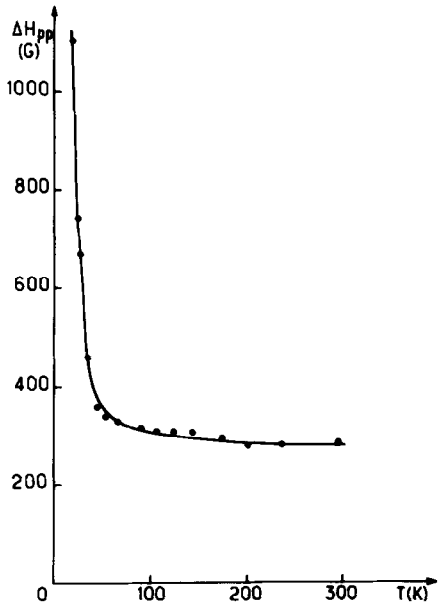

FIG. 3. The variation of EPR linewidth ΔH_{pp} as a function of temperature.

rical and has a Lorentzian shape. At room temperature the linewidth ΔH_{pp} = 290 G and g = 1.974. The variation of the linewidth as a function of temperature appears in Fig. 3.

Description of the Structure and Discussion

The projection of the structure on the (010) plane is given in Fig. 4. The anionic octahedral environment of the chromium atoms is slightly distorted, as shown in Table II. As can be expected this structure is exactly homologous to that of $K_2Ta_2O_3F_6$ with Cr taking the place of Ta and Pb the place of K (*1*).

The $(CrF_6)^{3-}$ octahedra share common corners (in a *cis* position) and form zig-zag chains $(CrF_5)_n^{2n-}$ parallel to the *b* axis. Two identical chains are linked together by common corners in the (101) plane and form thus a double chain $(Cr_2F_9)_n^{3n-}$ (Fig. 5). The potassium and lead atoms are between these chains and ensure the cohesion of the

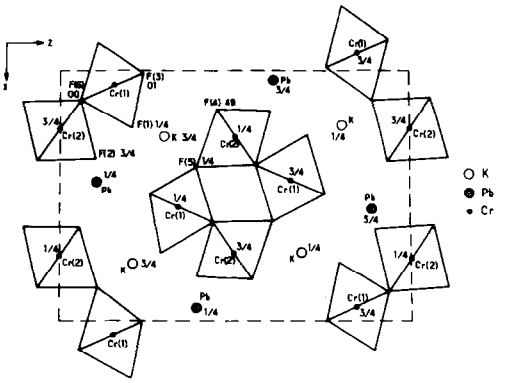

FIG. 4. Projection of the structure on the (010) plane.

lattice. Three of the fluorine atoms are found in bridging positions in the chains while the other three are in terminal positions. This situation is reflected in the differences of the observed Cr–F and F–F bond lengths.

The CrF_6 octahedra are only slightly distorted with average distances Cr(1)–F = 1.899 Å and Cr(2)–F = 1.898 Å for the two independent chromium atoms. These values compare well with the sum of ionic radii (1.895 Å) (*9*) and the average observed distances in $CaCrF_5$ (1.90 Å) (*10*) and

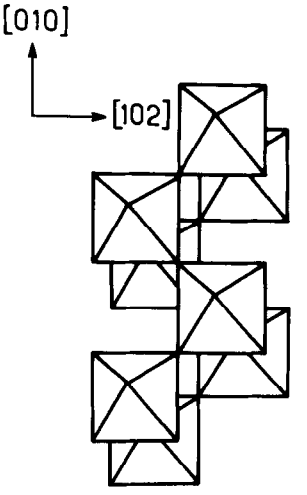

FIG. 5. Partial view of an infinite double chain $(Cr_2F_9)_n^{3n-}$. Octahedra in front are connected to those in back.

Rb_2CrF_5 (1.904 Å) (*11*). However, there is a clear difference between the terminal and bridging Cr–F distances. The average $Cr(1)–F_T$ = 1.877 Å and $Cr(2)–F_T$ = 1.881 Å bond lengths are clearly shorter than $Cr(1)–F_B$ = 1.920 Å and $Cr(2)–F_B$ = 1.915 Å. The same phenomenon was observed in other structures containing $M–F_T$- and $M–F_B$-type bonds, such as $CaCrF_5$ (*10*), Rb_2CrF_5 (*11*), and K_2FeF_5 (*5*).

This phenomenon can be explained by the competition in the $Cr(1)–F_B$ and $Cr(2)–F_B$ bonds, which weakens them mutually, and the absence of such competition in the bonds involving F_T. On the contrary, an opposite result is observed for $K_2Ta_2O_3F_6$, where the oxygen atoms are found in bridging positions and fluorine in terminal. In such a case we have $\langle Ta–O\rangle_B$ = 1.894 Å, much shorter than $\langle Ta–F\rangle_T$ = 1.952 Å. The discrepancy with the fluorides can be explained by the formation of strong covalent π-type bonds between the tantalum and oxygen atoms. The potassium and lead atoms are 9-coordinated with average K–F and Pb–F distances of 2.873 and 2.656 Å, respectively ($\Sigma r_{K,F}$ = 2.88 Å and $\Sigma r_{Pb,F}$ = 2.66 Å).

As can be seen from Fig. 1, the reciprocal susceptibility follows, in the temperature range 750–100 K, a Curie–Weiss law and leads to $\theta_p = -95$ K and $C_M = 1.98 \pm 0.03$ ($C_{theor.} = 1.875$, spin only). Below 100 K there is a flattening of the curve followed by an abrupt drop at very low temperature. The negative paramagnetic Curie temperature indicates a rather strong antiferromagnetic behavior. The double-chain-like character of the structure points to a certain anisotropy in the magnetic interactions, the strongest interactions being expected along the *b* axis (i.e., the double-chain direction). The flattening of the curve probably illustrates the predominance of those interactions.

The thermal variation of the EPR linewidth (Fig. 3) allows one to determine the three-dimensional magnetic-ordering temperature. The curve is asymptotical to the vertical $T = T_N$ line, with T_N = 17 K. The temperature dependence in the range $0.1 < (1 - T_N/T) < 0.70$ follows a $\Delta H = \Delta H_0 (1 - T_N/T)^{\beta}$ law, with $\beta = 0.511$. This value is the sum of two contributions, one coming from the Gaussian decay (or short-time contribution) and the other corresponding to the long-time diffusive decay, which, for double chains, has not yet been worked out theoretically. The important difference between θ_p and T_N in $KPbCr_2F_9$ can only be indicative of a reduced dimensionality represented by a chain-like structure, since in 3D antiferromagnetic materials these values are normally of the same order of magnitude.

References

1. J. P. Chaminade, M. Vlasse, M. Pouchard, and P. Hagenmuller, *Bull. Soc. Chem.* **9–10,** 1791 (1974).
2. M. Vlasse, J. P. Chaminade, and M. Pouchard, *Bull. Soc. Fr. Mineral. Cristallogr.* **99,** 3 (1976).
3. M. Vlasse, F. Menil, C. Moriliere, J. M. Dance, A. Tressaud, and J. Portier, *J. Solid State Chem.* **17,** 291 (1976).
4. J. M. Dance, R. Sabatier, F. Menil, M. Wintenberger, J. C. Cousseins, G. Le Flem, and A. Tressaud, *Solid State Commun.* **19,** 1059 (1976).
5. M. Vlasse, G. Matejka, and A. Tressaud, *Acta Crystallogr. Sect. B* **33,** 3377 (1977).
6. W. R. Busing, K. O. Martin, and H. A. Levy, ORFLS Report ORLN-TM-305, Oak Ridge National Laboratory, Oak Ridge, Tenn. (1962).
7. W. H. McMaster, N. Ker Del Grande, J. H. Mallet, and J. H. Hubbel, "Compilation of X-Ray Cross Sections," National Bureau of Standards, UCRL-50174, Sect. II, Rev. 1 (1969).
8. D. T. Cromer, *Acta Crystallogr.* **18,** 17 (1965).
9. R. D. Shannon and C. T. Prewitt, *Acta Crystallogr. Sect. B* **25,** 925 (1969).
10. D. Dumora, R. Von Der Mühll, and J. Ravez, *Mater. Res. Bull.* **6,** 561 (1971).
11. C. Jacobini, R. De Pape, M. Poulain, J. Le Marouille, and D. Grandjean, *Acta Crystallogr. Sect. B* **30,** 2688 (1974).